

When New Generators Arrive: Lifelong Machine-Generated Text Attribution via Ridge Feature Transfer

Zhen Sun^{1,2,3*} Yifan Liao³ Zhicong Huang^{2†} Jiaheng Wei³
Cheng Hong² Yutao Yue^{3,4} Xinlei He^{1†}

¹Wuhan University ²Ant Group

³The Hong Kong University of Science and Technology (Guangzhou)

⁴Institute of Deep Perception Technology, JITRI

arXiv:2606.05626v1 [cs.CL] 4 Jun 2026

Abstract

Machine-generated text (MGT) attribution aims to identify the specific generator responsible for a given text, thereby providing fine-grained evidence for model accountability and misuse investigation. As new large language models continue to emerge, attribution models must continuously incorporate new generators while preserving their ability to recognize previously seen ones. Prior works have shown that this lifelong MGT attribution setting is challenging, and existing methods often struggle to achieve a stable balance between adapting to new classes and retaining old ones. To address this issue, we propose *RidgeFT*, a lightweight analytic update framework that does not rely on exemplar replay. *RidgeFT* trains a task-aware encoder on the initial generator set, stores compact class-wise sufficient statistics when each generator class is first observed, and then freezes the encoder for replay-free closed-form updates. It then suppresses generator-irrelevant variation through covariance calibration, improves representation capacity with fixed random features, and updates new classes through closed-form ridge regression based on class-level sufficient statistics. Across multi-topic evaluations with varying initial generator setups, *RidgeFT* consistently outperforms baselines. It achieves the best macro-F1 across domains, backbones, and incremental protocols, while also improving both old-class retention and new-class adaptation. These results suggest that feature-stable analytic updates provide a simple yet effective approach to lifelong MGT attribution.

1 Introduction

As generative tools powered by large language models (LLMs) become increasingly widespread [26, 27], users can now conveniently rely on them for text generation and polishing. While these capabilities improve writing efficiency, they also introduce potential risks of misuse [15]. For example, users may exploit LLMs to automatically produce large vol-

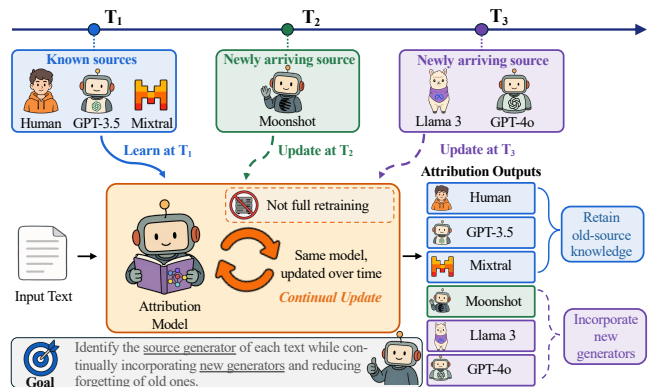


Figure 1: Illustration of the lifelong MGT attribution setting.

umes of papers, news articles, reviews, and other forms of text, thereby disrupting the normal order of content production and undermining the credibility of human-authored writing [38]. Against this backdrop, the effective identification of machine-generated text (MGT) has become an important problem. To address this issue, existing studies have primarily focused on two aspects of MGT identification: binary detection and source attribution [9, 38]. Compared with binary detection, MGT attribution further aims to identify the specific source generator, thereby providing finer-grained evidence for accountability tracking and misuse investigation [2].

Existing MGT attribution methods typically assume a fixed set of generators, which is often an unrealistic assumption in real-world settings. Since the attribution systems operate in a dynamic and open generator space in practice, they should not only recognize newly emerging generators, but also preserve the ability to distinguish previously seen ones. [21] introduces a more realistic setting, known as class-incremental MGT attribution, which we refer to as lifelong MGT attribution throughout this paper. Under this setting, the attribution model needs to be continuously updated as new generator classes arrive over time. However, due to factors such as computational cost, data licensing constraints, or the unavailability of historical data, it is usually impractical to recollect

*Work done during an internship at Ant Group.

†Corresponding authors: Zhicong Huang(zhicong.hzc@antgroup.com), Xinlei He(xinlei.he@whu.edu.cn).

all past data and retrain the model from scratch [11, 37]. At the same time, directly updating the model using only data from new classes often leads to catastrophic forgetting [5, 23]. Therefore, a central challenge in lifelong MGT attribution is efficiently incorporating new generator classes under limited data while maintaining stable recognition of previously learned generators.

Under this challenge, we posit that the difficulty of lifelong MGT attribution does not necessarily need to be addressed by continuously updating the entire text encoder. Instead, a task-tuned encoder trained on the initial set of generators can already capture strong generator-related representations. If this encoder continues to be fine-tuned during the incremental stage, the representation space will continue to shift as new classes arrive, thereby making the decision boundaries of old classes unstable [1, 40]. We therefore seek to decouple the learning of new generators from deep representation updating, ensuring that incremental knowledge is absorbed without altering or disrupting the stable representation space. Motivated by this idea, we propose *RidgeFT*, an exemplar-free analytic update framework for lifelong MGT attribution. We consider a practical deployment scenario where the attribution system is trained and maintained from the initial stage. During initialization, *RidgeFT* uses the initial-class data to train a task-aware encoder and construct compact class-wise sufficient statistics; after that, the raw texts of old classes are discarded and never replayed. When new generators arrive, *RidgeFT* keeps the encoder frozen, maps the new data through covariance calibration and fixed random features, accumulates the corresponding statistics, and updates the classifier by a closed-form ridge solution. In this way, incremental learning is performed through statistical memory rather than historical-text replay or repeated encoder fine-tuning. We evaluate *RidgeFT* in a multi-topic setting [21, 34], using P3, P4, and P5 protocols that start from 3, 4, and 5 initial classes and incrementally add 3, 2, and 1 new generator classes, respectively. Under the standard P5 protocol, *RidgeFT* achieves 0.886 full-F1, 0.902 old-class F1, and 0.804 new-class F1, improving full-F1 by 0.037 over the strongest continual-learning baseline.

Our contributions are summarized as follows:

- We identify lifelong MGT attribution as a generator-evolving attribution problem, where the model must preserve generator-specific decision boundaries while suppressing topic-, domain-, and prompt-induced nuisance variation under an exemplar-free update constraint.
- We propose *RidgeFT*, an exemplar-free analytic update framework that combines fractional covariance calibration, isotropic random feature lifting, and class-balanced closed-form ridge regression, enabling incremental updates using only compact class-wise sufficient statistics.
- We conduct extensive experiments across multiple topics, multiple target generators, and two backbones. The results show that *RidgeFT*'s main advantage lies in substantially improving new-generator adaptation while maintaining competitive old-generator retention.

2 Related Work

Establishing effective regulatory mechanisms for MGT has become essential for maintaining content credibility and supporting platform governance [38]. Recent research has pushed MGT detection from idealized binary classification toward more complex real-world scenarios. Studies have not only developed dynamic benchmarks accounting for multilingual settings and model evolution [22, 41], but also improved detector generalization to unseen generators and domains [3, 7, 14], alongside enhancing robustness against adversarial attacks [17, 18, 28]. Additionally, phenomena with blurred boundaries, such as human-AI collaborative writing, have fallen into the scope of platform monitoring [31, 33, 34]. However, although MGT detection techniques have made progress in addressing realistic challenges, merely determining whether a text is machine-generated is no longer sufficient to satisfy the growing demands for accountability tracing and copyright attribution.

Compared with binary detection, MGT attribution further requires identifying the specific generator responsible for a text, providing critical evidence for model accountability and forensic analysis [4, 9], and has emerged as an important branch of authorship attribution [10]. While prior studies have explored practical attribution settings [16, 25, 32], they mostly consider static scenarios where the candidate generator set is fixed. In real-world deployment, rapid LLM updates require attribution models to evolve accordingly to recognize new generators. Simultaneously, data privacy and licensing restrictions often prevent full retraining on historical data. To address this, [21] pioneered class-incremental MGT attribution and evaluated mainstream continual learning methods. Nevertheless, existing approaches still struggle to preserve recognition performance on previously seen generators while learning the characteristics of new ones. Breaking this trade-off between adaptation to new classes and retention of old ones in lifelong MGT attribution remains an unresolved challenge, which is the central problem addressed in this work.

3 Methodology

In lifelong MGT attribution, continuously fine-tuning the text encoder on new generators alters the representation geometry of old classes, thereby degrading previous decision boundaries. To address this, we propose *RidgeFT*, which reformulates lifelong attribution as an analytic ridge regression problem based on sufficient statistics. *RidgeFT* is designed for an attribution system that is trained and maintained from the initial stage, so the required statistics of initial classes can be recorded when those classes are first available. By freezing the base text encoder, *RidgeFT* preserves prior knowledge and performs analytic updates exclusively on the extracted features. Given an input text x , its frozen representation $h = f_{\theta}(x)$ is mapped to the final prediction via a novel sequential pipeline: covariance calibration, isotropic random feature lifting, and class-balanced ridge regression ($h \rightarrow \tilde{h} \rightarrow z(x) \rightarrow \hat{y}$). The calibration transform and the initial sufficient statistics are computed once from the base-stage training data and then stored. During later incremental stages,

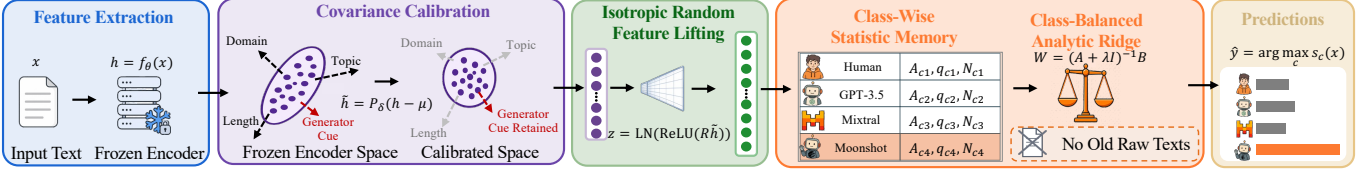


Figure 2: Overview of *RidgeFT*.

RidgeFT only processes newly arriving class data and does not revisit old raw texts.

Covariance Calibration. Base representations often capture generator-irrelevant variations (e.g., topic, length, domain) as high-variance directions, which impairs subsequent inner-product classifiers. To mitigate this, *RidgeFT* applies a fractional whitening transformation to suppress within-class noise while preserving the original discriminative geometry. This transform is estimated only from the base-stage training representations and is kept fixed after initialization, so incremental updates do not require replaying previous raw texts.

First, we calculate the within-class scatter matrix S_w :

$$S_w = \frac{1}{N - C_0} \sum_{c=1}^{C_0} \sum_{i:y_i=c} (h_i - \mu_c)(h_i - \mu_c)^\top, \quad (1)$$

where N is the total number of base samples, C_0 is the number of base classes, h_i is the representation of the i -th sample, and μ_c is the feature mean of class c . To address the instability of high-dimensional covariance estimation, we apply trace-scaled shrinkage:

$$S_w^{\text{shrink}} = (1 - \alpha)S_w + \alpha \frac{\text{tr}(S_w)}{d_h} I_{d_h}, \quad (2)$$

where α is the shrinkage parameter, $\text{tr}(\cdot)$ denotes the matrix trace, d_h is the feature dimension, and I_{d_h} is the identity matrix. Finally, we compute the fractionally whitened representation \tilde{h} via the eigenvalue decomposition of S_w^{shrink} :

$$S_w^{\text{shrink}} = U \Lambda U^\top, \Lambda = \text{diag}(\sigma_1, \dots, \sigma_{d_h}), \quad (3)$$

Given the eigendecomposition of S_w^{shrink} , we calibrate each principal direction according to its estimated within-class variance:

$$P_\delta = U(\Lambda + \varepsilon I_{d_h})^{-\delta} U^\top, \tilde{h} = P_\delta(h - \mu). \quad (4)$$

Here, U and Λ represent the eigenvectors and eigenvalues of S_w^{shrink} , respectively, with σ_j denoting the j -th eigenvalue. The parameter $\delta \in [0, 1]$ controls the whitening strength, μ is the global feature mean, and ε is a small constant ensuring numerical stability. By applying a fractional exponent instead of full whitening, we attenuate dominant within-class variations without excessively distorting the original feature space. This provides a stable input for the downstream analytic classifier. As exemplified in Figure 2, this calibration is intended to reduce nuisance directions associated with topic, length, and domain, while preserving generator-related cues for attribution.

Isotropic Random Feature Lifting. After covariance calibration, *RidgeFT* further lifts the calibrated representations

into a fixed nonlinear random feature space to boost the expressive capacity of the analytic classifier without sacrificing closed-form incremental updates. By adopting a non-trainable random mapping [29] instead of a learnable projection layer, we ensure the feature basis remains strictly invariant upon the arrival of new generators.

Let $\tilde{h} \in \mathbb{R}^{d_h}$ denote the calibrated encoder representation, where d_h is the feature dimension. *RidgeFT* samples a Gaussian random matrix $R \in \mathbb{R}^{d_\phi \times d_h}$ once before incremental learning, with each entry drawn independently as $R_{ij} \stackrel{\text{i.i.d.}}{\sim} \mathcal{N}(0, 1/d_h)$. The lifted feature is computed as

$$z(x) = \text{LN}(\text{ReLU}(R\tilde{h})) \in \mathbb{R}^{d_\phi}, \quad (5)$$

where d_ϕ is the random feature dimension and $\text{LN}(\cdot)$ denotes layer normalization. The matrix R is fixed throughout all incremental stages, so only the sufficient statistics of the ridge classifier need to be updated.

We use an isotropic Gaussian projection rather than a data-dependent projection learned from base classes. In lifelong MGT attribution, future generators may introduce variation directions that are not present in the initial generator set. A projection fitted to base-class geometry may therefore overemphasize existing class separations and reduce coverage of unseen generator-specific directions. By contrast, isotropic random features provide a task-agnostic nonlinear basis that expands the calibrated representation more uniformly, enabling the downstream ridge regressor to form richer decision boundaries without changing the representation space during continual learning.

Class-Balanced Analytic Ridge Regression. Using the random feature representation $z(x)$, *RidgeFT* trains the classification head via closed-form ridge regression. Because this analytic approach relies solely on second-order feature statistics, unlike iterative SGD-based methods, we only need to update the sufficient statistics for each class during the incremental stage, strictly eliminating the need to store raw text from old classes.

For each class c , *RidgeFT* stores only three sufficient statistics in the random feature space: the second-order statistic $A_c = \sum_{i:y_i=c} z_i z_i^\top$, the first-order statistic $q_c = \sum_{i:y_i=c} z_i$, and the sample count N_c . These statistics are computed when class c is first observed and are then retained as statistical memory, so later updates do not require replaying its raw texts. When a new generator arrives, *RidgeFT* only computes the same statistics for the new class and appends them to the existing table. However, directly summing class statistics can bias the ridge solution toward classes with larger sample counts, since both A_c and q_c scale with N_c . To reduce this imbalance, *RidgeFT* introduces inverse-frequency weights based on class

sample counts:

$$\omega_c = \frac{(N_c + \tau)^{-\beta}}{\frac{1}{|\mathcal{Y}_t|} \sum_{c' \in \mathcal{Y}_t} (N_{c'} + \tau)^{-\beta}}, \quad c \in \mathcal{Y}_t, \quad (6)$$

where \mathcal{Y}_t is the set of classes observed up to incremental stage t , β controls the strength of reweighting, and τ prevents small classes from receiving excessively large weights. We then construct the ridge regression solution using the weighted statistics. Specifically, let $\bar{A} = \sum_{c \in \mathcal{Y}_t} \omega_c A_c$, and let the c -th column of \bar{B} be $\omega_c q_c$. The final classifier is given by

$$W = (\bar{A} + \lambda I_{d_\phi})^{-1} \bar{B}, \quad (7)$$

where $\lambda > 0$ is the ridge regularization coefficient.

By mitigating the dominance of majority classes via reweighting, *RidgeFT* converts incremental updates into the simple accumulation of sufficient statistics and a single linear system solve. This enables the efficient absorption of new generators without encoder drift. At inference, the model predicts the class maximizing $s(x) = z(x)^\top W$. Algorithm 1 summarizes this overall procedure.

Algorithm 1 *RidgeFT* Update

Require: Frozen encoder f_θ , calibration transform P_δ , random matrix R , streams $\{\mathcal{D}_t\}_{t=0}^T$

Ensure: Ridge classifier W

- 1: Initialize seen classes $\mathcal{Y}_{-1} \leftarrow \emptyset$ and statistics $\{A_c, q_c, N_c\}$ as empty.
 - 2: **for** $t = 0, \dots, T$ **do**
 - 3: $\mathcal{Y}_t \leftarrow \mathcal{Y}_{t-1}$.
 - 4: **for each** $(x_i, y_i) \in \mathcal{D}_t$ **do**
 - 5: **if** $y_i \notin \mathcal{Y}_t$ **then**
 - 6: Add y_i to \mathcal{Y}_t and initialize $A_{y_i}, q_{y_i}, N_{y_i}$ as zero.
 - 7: **end if**
 - 8: $z_i \leftarrow \text{LN}(\text{ReLU}(RP_\delta(f_\theta(x_i) - \mu)))$.
 - 9: $A_{y_i} \leftarrow A_{y_i} + z_i z_i^\top, \quad q_{y_i} \leftarrow q_{y_i} + z_i, \quad N_{y_i} \leftarrow N_{y_i} + 1$.
 - 10: **end for**
 - 11: $\omega_c \leftarrow \frac{(N_c + \tau)^{-\beta}}{|\mathcal{Y}_t|^{-1} \sum_{c' \in \mathcal{Y}_t} (N_{c'} + \tau)^{-\beta}}, \quad \forall c \in \mathcal{Y}_t$.
 - 12: $\bar{A} \leftarrow \sum_{c \in \mathcal{Y}_t} \omega_c A_c, \quad \bar{B} \leftarrow [\omega_c q_c]_{c \in \mathcal{Y}_t}$.
 - 13: $W \leftarrow (\bar{A} + \lambda I_{d_\phi})^{-1} \bar{B}$.
 - 14: **end for**
 - 15: **return** W
-

4 Experimental Setting

Task Protocol. To simulate the continual emergence of generators in real-world scenarios, we adopt a class-incremental MGT attribution benchmark targeting 1 Human source and 5 LLMs. We evaluate our method under 3 incremental protocols: P3, P4, and P5, which begin with 3, 4, and 5 initial classes, respectively. While P5 follows the standard single-step incremental setting of prior work [21], P3 and P4 are introduced to further increase task difficulty. By starting with smaller base sets and introducing one new class per subsequent step, P3 and P4 involve more incremental stages,

thereby imposing substantially stricter requirements on the model’s resistance to catastrophic forgetting.

Dataset. We conduct experiments on two representative benchmark datasets, which correspond to two major real-world scenarios where LLM misuse poses particularly significant risks: rigorous academic writing and diverse social media interaction. (1) MGT-Academic [21]: This dataset focuses on the academic writing domain and covers three disciplines, namely STEM, Humanities, and Social Science. It includes human-authored text as well as text generated by five mainstream models, namely GPT-3.5¹, GPT-4o-mini [12], Moonshot [24], Mixtral-8x7B [13], and Llama-3.1 [6]. We use the full dataset in our experiments, which contains approximately 73K samples in total. (2) AIGTBench (Social Media Subset) [34]: The texts in this subset are drawn from major social media platforms. It likewise contains human-written text and text generated by GPT-3.5, GPT-4o-mini, Llama-1 [35], Llama-2 [36], and Llama-3.1. To ensure rigorous evaluation and class balance, we uniformly sample 15K instances from each class for our experiments.

Baselines & Implementation. We follow the experimental protocol of [21] and compare our method against several representative baselines. We include the classical methods LwF [19], iCaRL [30], and BiC [39], as well as the more recent EASE [43], PASS [44] and SimpleCIL [42]. To ensure fair comparison, all replay-based methods use the same memory buffer setting, with 100 stored samples for each old class. As for the backbone, we adopt DeBERTa-v3-base [8] and RoBERTa-base [20] as the text encoders for feature extraction.

Evaluation Metrics. All experiments are conducted under the same data splits, incremental protocols, and memory budget. As the primary evaluation metric, we use macro-F1. To provide a more detailed analysis of model behavior, we report not only the overall macro-F1 over all seen classes, but also separate scores on old classes and new classes. This multi-dimensional evaluation enables us to quantify how different methods balance two competing objectives: mitigating catastrophic forgetting on old classes and adapting to newly introduced ones. Unless otherwise specified, we report the mean performance over three random seeds.

5 Experiments

5.1 Comparison with Baselines

We compare *RidgeFT* with a wide range of baselines under 3 evaluation protocols. Baselines marked with *, such as LwF*, iCaRL*, BiC*, and EASE*, denote methods equipped with a replay mechanism that stores historical samples.

As shown in Figures 3 and 6, *RidgeFT* consistently outperforms all baselines across the P3 and P4 incremental stages in both domains. In the academic setting, encompassing the STEM, Humanities, and Social Science datasets, under P3 (sequentially adding Moonshot, Llama-3.1, and GPT-4o-mini), *RidgeFT* maintains strong old-class F1 (0.913, 0.870, 0.861) and new-class F1 (0.814, 0.729, 0.799) across the three stages.

¹<https://openai.com/index/chatgpt>.

Table 1: Performance Comparison across Domains and Models. * denotes methods using data replay. “Ori.” denotes the original base-stage model before incremental updating, i.e., the S0 performance on the initial generator classes, and is reported only as a reference rather than as a continual-learning baseline. Darker color indicates better performance. Bold values indicate the best result among continual-learning methods within each backbone block.

Domain	New Model	RoBERTa-base								DeBERTa-base							
		Ori.	LwF*	iCaRL*	BiC*	EASE*	PASS	SimpleCIL	<i>RidgeFT</i> (Ours)	Ori.	LwF*	iCaRL*	BiC*	EASE*	PASS	SimpleCIL	<i>RidgeFT</i> (Ours)
Social Science	GPT-3.5	0.906	0.833	0.845	0.835	0.844	0.772	0.769	0.865	0.891	0.819	0.812	0.801	0.753	0.780	0.765	0.851
	Mixtral	0.938	0.845	0.837	0.851	0.845	0.801	0.771	0.880	0.938	0.841	0.830	0.833	0.758	0.785	0.773	0.878
	Moonshot	0.931	0.847	0.843	0.840	0.816	0.780	0.792	0.868	0.922	0.835	0.829	0.827	0.788	0.784	0.778	0.862
	Llama-3.1	0.920	0.820	0.806	0.814	0.811	0.761	0.751	0.854	0.912	0.785	0.790	0.784	0.753	0.750	0.739	0.853
	GPT-4o-mini	0.905	0.830	0.810	0.838	0.810	0.768	0.790	0.868	0.898	0.834	0.823	0.823	0.829	0.795	0.765	0.867
	Average	0.920	0.835	0.828	0.836	0.825	0.777	0.775	0.867	0.912	0.823	0.817	0.814	0.776	0.779	0.764	0.862
STEM	GPT-3.5	0.946	0.882	0.880	0.883	0.867	0.802	0.805	0.914	0.942	0.847	0.850	0.855	0.847	0.808	0.801	0.907
	Mixtral	0.964	0.887	0.883	0.878	0.874	0.830	0.809	0.912	0.966	0.879	0.877	0.875	0.867	0.813	0.822	0.919
	Moonshot	0.959	0.895	0.880	0.891	0.885	0.841	0.830	0.916	0.958	0.893	0.885	0.888	0.892	0.834	0.853	0.917
	Llama-3.1	0.959	0.852	0.844	0.851	0.757	0.809	0.801	0.902	0.956	0.860	0.852	0.852	0.856	0.809	0.822	0.910
	GPT-4o-mini	0.942	0.888	0.882	0.885	0.780	0.826	0.827	0.913	0.945	0.854	0.862	0.890	0.888	0.837	0.831	0.919
	Average	0.954	0.881	0.874	0.878	0.832	0.822	0.814	0.911	0.953	0.867	0.865	0.872	0.870	0.820	0.826	0.914
Humanities	GPT-3.5	0.903	0.854	0.856	0.831	0.863	0.816	0.780	0.881	0.898	0.827	0.824	0.834	0.826	0.787	0.768	0.873
	Mixtral	0.954	0.856	0.854	0.851	0.850	0.817	0.805	0.876	0.952	0.831	0.828	0.838	0.832	0.803	0.791	0.870
	Moonshot	0.936	0.851	0.840	0.843	0.844	0.779	0.807	0.862	0.945	0.825	0.829	0.841	0.823	0.789	0.814	0.872
	Llama-3.1	0.928	0.809	0.800	0.806	0.810	0.771	0.771	0.851	0.922	0.701	0.787	0.795	0.789	0.739	0.768	0.856
	GPT-4o-mini	0.903	0.843	0.836	0.848	0.838	0.799	0.771	0.868	0.905	0.830	0.747	0.830	0.806	0.806	0.730	0.868
	Average	0.925	0.843	0.837	0.836	0.841	0.796	0.787	0.867	0.924	0.803	0.803	0.828	0.815	0.785	0.774	0.868
AIGTBench	GPT-3.5	0.964	0.875	0.870	0.876	0.863	0.840	0.804	0.894	0.959	0.873	0.847	0.863	0.851	0.833	0.814	0.892
	GPT-4o-mini	0.956	0.823	0.833	0.866	0.800	0.855	0.820	0.896	0.954	0.798	0.835	0.834	0.802	0.815	0.803	0.889
	Llama-1	0.913	0.892	0.867	0.897	0.896	0.851	0.878	0.915	0.916	0.881	0.870	0.873	0.873	0.845	0.794	0.910
	Llama-2	0.918	0.856	0.817	0.855	0.837	0.795	0.775	0.892	0.919	0.844	0.840	0.856	0.844	0.794	0.811	0.893
	Llama-3.1	0.915	0.864	0.842	0.856	0.837	0.836	0.777	0.899	0.913	0.841	0.762	0.840	0.837	0.796	0.796	0.895
	Average	0.933	0.862	0.846	0.870	0.847	0.835	0.811	0.899	0.932	0.848	0.831	0.853	0.842	0.817	0.804	0.896
Overall Average	0.933	0.855	0.846	0.855	0.836	0.807	0.797	0.886	0.930	0.835	0.829	0.842	0.826	0.800	0.792	0.885	

Under P4, it achieves full-F1 scores of 0.862 and 0.838, significantly outpacing the strongest baseline, which drops from 0.797 to 0.730. This highlights that replay-based baselines still struggle to balance old and new classes, while replay-free baselines such as PASS and SimpleCIL are even more limited when generator classes arrive sequentially. This robust advantage extends to the social media setting, where *RidgeFT* sustains high full-F1 scores across the P3 stages (0.945, 0.868, 0.855) and P4 stages (0.878, 0.867). Notably, at the final social media P4 stage, *RidgeFT*’s new-class F1 reaches 0.899, substantially beating the strongest baseline (0.735). These results confirm that *RidgeFT* remains stable absorbing continuous generator arrivals without compromising past knowledge.

This advantage is further confirmed under the P5 protocol (refer to Table 1). Averaged over the two backbones, *RidgeFT* achieves 0.886 full-F1, 0.902 old-class F1, and 0.804 new-class F1. Compared with the strongest full-F1 baseline, it improves full-F1 by 0.037. Compared with the best baseline on new-class F1, it improves new-class F1 by 0.107, while also outperforming the best old-class baseline on old-class F1. This reveals a core limitation of baselines: they are better at preserving the decision boundaries of previously learned features, yet remain less effective at efficiently absorbing information from new classes. In contrast, *RidgeFT* not only performs better in retaining old classes, but also delivers a substantial improvement on the more critical task of recognizing new classes, surpassing the strongest baseline by 0.107.

Finally, using GPT-4o-mini as the target generator (STEM / DeBERTa-base / P5), we analyze the impact of target-class data proportions. As shown in Figure 4, when reducing target-class data from 100% to 5%, *RidgeFT*’s full-F1 remains highly stable (ranging from 0.919 to 0.908). Conversely, the

strongest replay baseline (LwF*) averages only 0.893, and the replay-free SimpleCIL drops to 0.831. This confirms that *RidgeFT* does not rely on abundant new-class data, demonstrating superior data efficiency and robustness even under severe low-resource incremental conditions.

5.2 Ablation Studies

Table 2: Component ablation of *RidgeFT* under different new-class data ratios. W denotes whitening, RFL denotes random feature lift, and CBR denotes class-balanced ridge. “Full” denotes full macro-F1 over all seen classes, while “New” denotes new-class F1.

Ratio	Only W		Only RFL		Only CBR		<i>RidgeFT</i>	
	Full	New	Full	New	Full	New	Full	New
20%	0.881	0.741	0.887	0.763	0.912	0.865	0.918	0.878
40%	0.904	0.830	0.908	0.839	0.912	0.865	0.919	0.880
60%	0.909	0.851	0.913	0.861	0.913	0.865	0.919	0.881
80%	0.912	0.861	0.916	0.872	0.912	0.865	0.919	0.880
100%	0.910	0.858	0.917	0.878	0.912	0.863	0.919	0.881

Component-wise Ablation. We ablate the 3 core components of *RidgeFT* using GPT-4o-mini as the target generator (STEM / DeBERTa-base / P5). As shown in Table 2, each component contributes distinctly, and they are highly complementary. When Whitening is used alone, the model can stabilize encoder features to some extent, but its adaptability remains limited under low-resource conditions. For example, with only 20% of the new-class data, the new-class F1 reaches only 0.741. In contrast, Random Feature Lift consistently outperforms Whitening across all data ratios, indicating that random nonlinear features enhance the separability of different generators. Class-Balanced Ridge (CBR) is the strongest

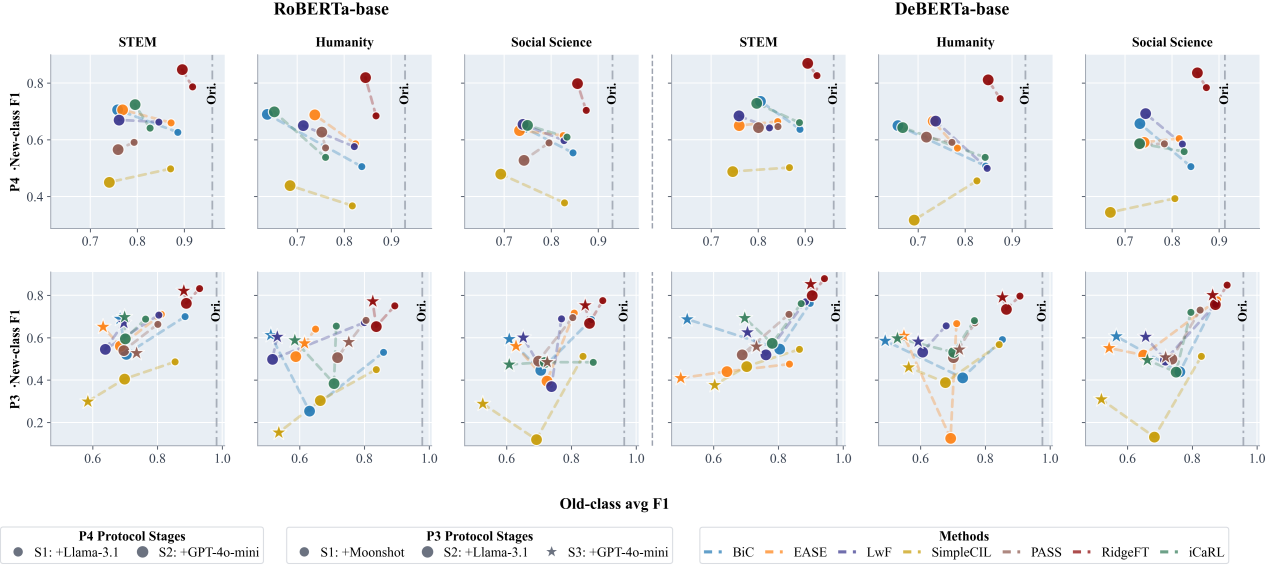


Figure 3: Experiments on academic topics. P3 starts with 3 initial classes and sequentially adds Moonshot, Llama-3.1, and GPT-4o-mini; P4 starts with 4 initial classes and sequentially adds Llama-3.1 and GPT-4o-mini.

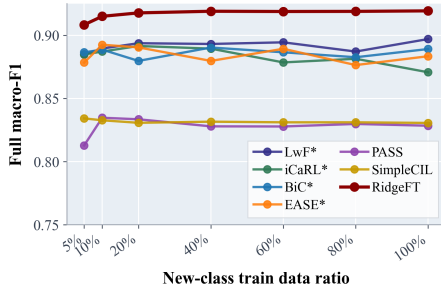


Figure 4: Full-F1 under varying target-class data proportions.

individual component. Even with only 20% of the data, it achieves a new-class F1 of 0.865, suggesting that it plays a central role in mitigating the bias between old and new classes. Notably, both CBR and the full *RidgeFT* exhibit stability across data ratios ranging from 20% to 100%. According to Equation (6), when $\beta = 1$ and $\tau = 0$, the class weight satisfies $\omega_c \propto 1/N_c$, which exactly offsets the linear growth of class statistics (A_c, q_c) with respect to the sample size N_c . Consequently, the ridge update effectively operates on class-averaged statistics, rendering the model largely insensitive to the sampling ratio once stable estimation is reached. Finally, combining all three components yields the best overall performance. Their complementarity is particularly evident in the 20% low-resource setting, where the full *RidgeFT* boosts the new-class F1 from 0.865 (CBR alone) to 0.878. Additional frozen-representation analysis is provided in Section A.

Parameter Sensitivity Ablation. Figure 5 presents the hyperparameter sensitivity of *RidgeFT*. Overall, it exhibits strong robustness to most hyperparameters. For example, varying the smoothing constant τ and the ridge regularization coefficient λ causes almost no performance fluctuation, with Full-F1 remaining consistently around 0.919. From the perspective of feature stabilization, a moderate amount of trace shrinkage,

with $\alpha \in [0.05, 0.10]$, is already sufficient to ensure reliable covariance estimation. The covariance calibration exponent δ performs best in the range $[0.375, 0.625]$, with Full-F1 reaching 0.919 at $\delta = 0.5$. However, overly strong calibration, such as $\delta = 1.0$, instead suppresses useful discriminative information in the features and leads to a performance drop. In terms of performance gains, the random feature dimension d_ϕ and the class reweighting strength β play the most important roles. As d_ϕ increases from 512 to 8192, the higher-dimensional feature space substantially improves the separability of new generators, steadily raising Full-F1 and new-class F1 to 0.9201 and 0.890, respectively. In addition, under the low-resource setting with 20% data, strong reweighting with $\beta = 1.0$ boosts new-class F1 by nearly 12 percentage points compared with the unweighted case $\beta = 0$, increasing it from 0.760 to 0.878. This highlights its decisive role in alleviating the severe imbalance between old and new classes.

Table 3: Sufficient-statistic compression ablation (default setting: $d_\phi = 4096$, 6 classes). Per-class schemes retain update flexibility, while merged schemes minimize storage by assuming future updates only add new classes, not new samples to old ones.

Storage scheme	Stored A statistics	Storage	Compression	Full-F1
fp64 baseline	$6 \times A_c$ in fp64	782.35 MiB	1.00×	0.919
fp32 per-class	$6 \times A_c$ in fp32	398.35 MiB	1.96×	0.919
bf16 per-class	$6 \times A_c$ in bf16	206.35 MiB	3.79×	0.920
merged fp32	$1 \times \bar{A}$ in fp32	78.35 MiB	9.99×	0.919
merged bf16	$1 \times \bar{A}$ in bf16	46.35 MiB	16.9×	0.920

Sufficient-Statistic Compression Ablation. Although *RidgeFT* is exemplar-free, it is not memory-free. Its closed-form update still requires storing the statistics needed for ridge regression: the calibration parameters, the fixed projection matrix R , and the class-wise sufficient statistics A_c, q_c , and N_c . The high-dimensional $A_c \in \mathbb{R}^{d_\phi \times d_\phi}$ dominates this storage cost. Under the default setting ($d_\phi = 4096$, 6 classes), the fp64 implementation requires 782.35 MiB in total, with the

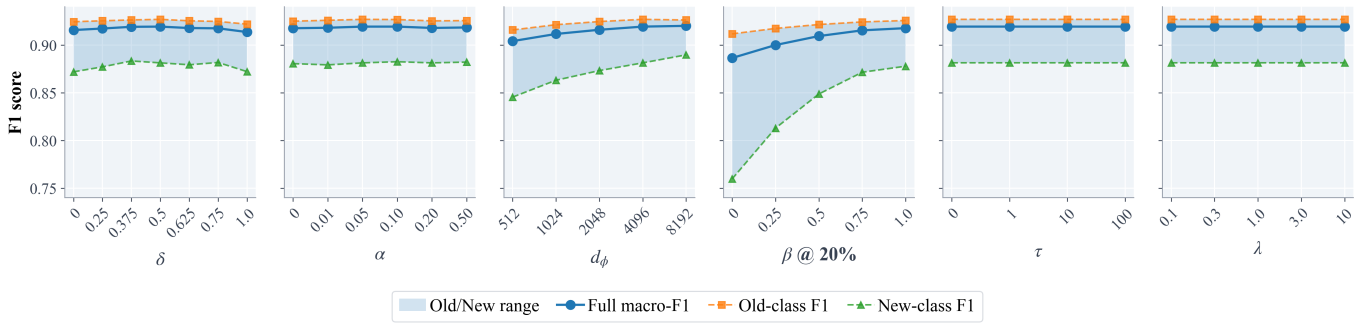


Figure 5: Parameter sensitivity of *RidgeFT*. We vary one hyperparameter at a time while keeping the others fixed, including the covariance calibration exponent δ , trace shrinkage coefficient α , random feature dimension d_ϕ , class-reweighting strength β under the 20% setting, smoothing constant τ , and ridge regularization coefficient λ .

six class-specific A_c matrices alone accounting for 768 MiB.

To reduce this bottleneck, we examine compression along two orthogonal dimensions. The first is numerical precision (fp32 or bf16), which preserves the full class-wise statistic table. This retains the flexibility to reweight classes post-training or incorporate new samples into previously seen classes. The second is class aggregation, which stores only the weighted merged matrix $\bar{A} = \sum_c \omega_c A_c$. This significantly reduces the memory footprint but folds the current class weights into the matrix, sacrificing the ability to update old classes individually. Importantly, this limitation is fully compatible with our P3/P4/P5 protocols, where incremental stages only introduce new generator classes.

As shown in Table 3, *RidgeFT* is highly robust to low-precision storage. Reducing per-class A_c to fp32 or bf16 substantially cuts storage while keeping the Full-F1 consistently above 0.919. Class aggregation yields even larger gains by removing redundant class-specific matrices. Among all variants, merged bf16 provides the optimal trade-off: it requires only 46.35 MiB (a 16.9 \times compression ratio) while achieving a Full-F1 of 0.920. Overall, *RidgeFT* should be viewed as replay-free rather than storage-free. Merged bf16 is the most compact choice for our new-class-only protocols, whereas per-class bf16 is preferable if future updates may add samples to old classes.

6 Conclusion

This paper addresses the challenge of lifelong MGT attribution: continuously learning new generators without suffering catastrophic forgetting or relying on historical text replay. To overcome the dilemma between representation drift (from fine-tuning) and memory overhead (from exemplars), we propose *RidgeFT*. By freezing a task-tuned encoder and formulating incremental adaptation as closed-form ridge regression, our replay-free framework balances old and new classes without encoder parameter updates. Extensive experiments confirm that *RidgeFT* achieves a superior trade-off against baselines, demonstrating that combining stable representations with analytic updates offers a scalable path for future MGT attribution systems.

Limitations

Although *RidgeFT* achieves strong performance in lifelong MGT attribution, it still has several limitations.

- **Storage Requirements and Compression:** *RidgeFT* is replay-free rather than completely storage-free. In other words, although it does not require storing raw text samples from old classes, its closed-form ridge updates still rely on storing the covariance calibration parameters, the fixed random projection matrix, and the class-level sufficient statistics. While our compression study shows that the storage cost can be substantially reduced through low-precision storage and statistical merging, how to further compress these statistical quantities remains an important direction for future research.
- **Multilingual Extension:** Our experiments are mainly conducted on English datasets. Since *RidgeFT* operates in the encoder representation space rather than relying on language-specific surface-level textual features, we believe that it has the potential to extend to multilingual MGT attribution. A natural direction for future work is to combine *RidgeFT* with multilingual encoders and systematically evaluate its effectiveness across more languages and cross-lingual generator settings.
- **Long-term Deployment and Representation Stability:** Because *RidgeFT* does not continue updating the deep encoder during the incremental stage, but instead relies on a fixed representation space, a fixed random feature mapping, and closed-form ridge updates, it should not be interpreted as a method that can absorb an unlimited number of new generators over an arbitrarily long time horizon without performance degradation. As future generators become increasingly different from those seen during the initial training stage, the frozen representation may contain insufficient generator-specific information, which can weaken the effectiveness of later incremental updates. Therefore, in longer-term deployment scenarios, an important open question is how to introduce periodic encoder adaptation or calibration refresh while preserving representation stability.

Ethical Considerations

This work focuses on lifelong machine-generated text attribution under benchmark settings. It does not collect private user data, involve human subjects, or introduce new generative or attack capabilities. The main potential risk lies in the deployment of attribution systems: imperfect predictions may cause incorrect judgments about the source of a text. Therefore, we suggest that MGT attribution models should be used as auxiliary evidence rather than as the sole basis for high-stakes decisions. Real-world deployment should further consider domain shift, transparency, and human oversight.

References

- [1] Lucas Caccia, Rahaf Aljundi, Nader Asadi, Tinne Tuytelaars, Joelle Pineau, and Eugene Belilovsky. New insights on reducing abrupt representation change in online continual learning. *arXiv preprint arXiv:2104.05025*, 2021. 2
- [2] Lucio La Cava and Andrea Tagarelli. Openturingbench: An open-model-based benchmark and framework for machine-generated text detection and attribution. In *Conference on Empirical Methods in Natural Language Processing (EMNLP)*, pages 26655–26671. Association for Computational Linguistics, 2025. 1
- [3] Zhihui Chen, Kai He, Yucheng Huang, Yunxiao Zhu, and Mengling Feng. Divscore: Zero-shot detection of llm-generated text in specialized domains. In Christos Christodoulopoulos, Tanmoy Chakraborty, Carolyn Rose, and Violet Peng, editors, *Conference on Empirical Methods in Natural Language Processing (EMNLP)*, pages 19231–19253. ACL, 2025. 2
- [4] Hongchao Fang, Yixin Liu, Jiangshu Du, Can Qin, Ran Xu, Feng Liu, Lichao Sun, Dongwon Lee, Lifu Huang, and Wenpeng Yin. Could ai trace and explain the origins of ai-generated images and text? *arXiv preprint arXiv:2504.04279*, 2025. 2
- [5] Robert M French. Catastrophic forgetting in connectionist networks. *Trends in cognitive sciences*, 3(4):128–135, 1999. 2
- [6] Aaron Grattafiori, Abhimanyu Dubey, Abhinav Jauhri, Abhinav Pandey, Abhishek Kadian, Ahmad Al-Dahle, Aiesha Letman, Akhil Mathur, Alan Schelten, Alex Vaughan, et al. The llama 3 herd of models. *arXiv preprint arXiv:2407.21783*, 2024. 4
- [7] Wei Hao, Ran Li, Weiliang Zhao, Junfeng Yang, and Chengzhi Mao. Learning to rewrite: Generalized llm-generated text detection. In Wanxiang Che, Joyce Nabende, Ekaterina Shutova, and Mohammad Taher Pilehvar, editors, *Annual Meeting of the Association for Computational Linguistics (ACL)*, pages 6421–6434. ACL, 2025. 2
- [8] Pengcheng He, Jianfeng Gao, and Weizhu Chen. Debertav3: Improving deberta using electra-style pre-training with gradient-disentangled embedding sharing. *arXiv preprint arXiv:2111.09543*, 2021. 4
- [9] Xinlei He, Xinyue Shen, Zeyuan Chen, Michael Backes, and Yang Zhang. Mgtbench: Benchmarking machine-generated text detection. In Bo Luo, Xiaojing Liao, Jun Xu, Engin Kirda, and David Lie, editors, *ACM SIGSAC Conference on Computer and Communications Security (CCS)*, pages 2251–2265. ACM, 2024. 1, 2
- [10] Baixiang Huang, Canyu Chen, and Kai Shu. Authorship attribution in the era of llms: Problems, methodologies, and challenges. *ACM SIGKDD Explorations Newsletter*, 26(2):21–43, 2025. 2
- [11] Jianheng Huang, Leyang Cui, Ante Wang, Chengyi Yang, Xinting Liao, Linfeng Song, Junfeng Yao, and Jinsong Su. Mitigating catastrophic forgetting in large language models with self-synthesized rehearsal. In *Annual Meeting of the Association for Computational Linguistics (ACL)*, pages 1416–1428, 2024. 2
- [12] Aaron Hurst, Adam Lerer, Adam P Goucher, Adam Perelman, Aditya Ramesh, Aidan Clark, AJ Ostrow, Akila Welihinda, Alan Hayes, Alec Radford, et al. Gpt-4o system card. *arXiv preprint arXiv:2410.21276*, 2024. 4
- [13] Albert Q Jiang, Alexandre Sablayrolles, Antoine Roux, Arthur Mensch, Blanche Savary, Chris Bamford, Devendra Singh Chaplot, Diego de las Casas, Emma Bou Hanna, Florian Bressand, et al. Mixtral of experts. *arXiv preprint arXiv:2401.04088*, 2024. 4
- [14] Kaijie Jiao, Quan Wang, Licheng Zhang, Zikang Guo, and Zhendong Mao. M-rangedetector: Enhancing generalization in machine-generated text detection through multi-range attention masks. In Wanxiang Che, Joyce Nabende, Ekaterina Shutova, and Mohammad Taher Pilehvar, editors, *Findings of the Association for Computational Linguistics: ACL*, pages 8971–8983. ACL, 2025. 2
- [15] Tharindu Kumarage, Garima Agrawal, Paras Sheth, Raha Moraffah, Aman Chadha, Joshua Garland, and Huan Liu. A survey of ai-generated text forensic systems: Detection, attribution, and characterization. *arXiv preprint arXiv:2403.01152*, 2024. 1
- [16] Lucio La Cava, Dominik Macko, Róbert Móra, Ivan Srba, and Andrea Tagarelli. Authorship attribution in multilingual machine-generated texts. *arXiv preprint arXiv:2508.01656*, 2025. 2
- [17] Xiang Li, Zhiyi Yin, Hexiang Tan, Shaoling Jing, Du Su, Yi Cheng, Huawei Shen, and Fei Sun. Prdetect: Perturbation-robust llm-generated text detection based on syntax tree. In Luis Chiruzzo, Alan Ritter, and Lu Wang, editors, *Findings of the Association for Computational Linguistics: NAACL*, pages 8290–8301. ACL, 2025. 2
- [18] Yuanfan Li, Zhaohan Zhang, Chengzhengxu Li, Chao Shen, and Xiaoming Liu. Iron sharpens iron: Defending

- against attacks in machine-generated text detection with adversarial training. In Wanxiang Che, Joyce Nabende, Ekaterina Shutova, and Mohammad Taher Pilehvar, editors, *Annual Meeting of the Association for Computational Linguistics (ACL)*, pages 3091–3113. ACL, 2025. 2
- [19] Zhizhong Li and Derek Hoiem. Learning without forgetting. *IEEE transactions on pattern analysis and machine intelligence*, 40(12):2935–2947, 2017. 4
- [20] Yinhan Liu, Myle Ott, Naman Goyal, Jingfei Du, Mandar Joshi, Danqi Chen, Omer Levy, Mike Lewis, Luke Zettlemoyer, and Veselin Stoyanov. Roberta: A robustly optimized bert pretraining approach. *arXiv preprint arXiv:1907.11692*, 2019. 4
- [21] Yule Liu, Zhiyuan Zhong, Yifan Liao, Zhen Sun, Jingyi Zheng, Jiaheng Wei, Qingyuan Gong, Fenghua Tong, Yang Chen, Yang Zhang, and Xinlei He. On the generalization and adaptation ability of machine-generated text detectors in academic writing. In *ACM SIGKDD Conference on Knowledge Discovery and Data Mining (KDD)*, pages 5674–5685. ACM, 2025. 1, 2, 4, 11
- [22] Dominik Macko, Jakub Kopal, Róbert Móra, and Ivan Srba. Multisocial: Multilingual benchmark of machine-generated text detection of social-media texts. In Wanxiang Che, Joyce Nabende, Ekaterina Shutova, and Mohammad Taher Pilehvar, editors, *Annual Meeting of the Association for Computational Linguistics (ACL)*, pages 727–752. ACL, 2025. 2
- [23] Michael McCloskey and Neal J Cohen. Catastrophic interference in connectionist networks: The sequential learning problem. In *Psychology of learning and motivation*, volume 24, pages 109–165. Elsevier, 1989. 2
- [24] Moonshot AI. Moonshot AI. <https://www.moonshot.ai/>, 2026. Accessed: 2026-05-15. 4
- [25] Ayat A Najjar, Huthaifa I Ashqar, Omar Darwish, and Eman Hammad. Leveraging explainable ai for llm text attribution: Differentiating human-written and multiple llm-generated text. *Information*, 16(9):767, 2025. 2
- [26] OpenClaw. Openclaw docs. <https://docs.openclaw.ai/>, 2026. Accessed: 2026-05-14. 1
- [27] Adetoun A Oyelude. Artificial intelligence (ai) tools for academic research. *Library Hi Tech News*, 41(8):18–20, 2024. 1
- [28] Andrea Pedrotti, Michele Papucci, Cristiano Ciaccio, Alessio Miaschi, Giovanni Puccetti, Felice Dell’Orletta, and Andrea Esuli. Stress-testing machine generated text detection: Shifting language models writing style to fool detectors. In Wanxiang Che, Joyce Nabende, Ekaterina Shutova, and Mohammad Taher Pilehvar, editors, *Findings of the Association for Computational Linguistics: ACL*, pages 3010–3031. Association for Computational Linguistics, 2025. 2
- [29] Ali Rahimi and Benjamin Recht. Random features for large-scale kernel machines. *Advances in neural information processing systems*, 20, 2007. 3
- [30] Sylvestre-Alvise Rebuffi, Alexander Kolesnikov, Georg Sperl, and Christoph H Lampert. icarl: Incremental classifier and representation learning. In *Proceedings of the IEEE conference on Computer Vision and Pattern Recognition*, pages 2001–2010, 2017. 4
- [31] Shoumik Saha and Soheil Feizi. Almost ai, almost human: The challenge of detecting ai-polished writing. In Wanxiang Che, Joyce Nabende, Ekaterina Shutova, and Mohammad Taher Pilehvar, editors, *Findings of the Association for Computational Linguistics: ACL*, pages 25414–25431. ACL, 2025. 2
- [32] Areg Mikael Sarvazyan, José Ángel González, Marc Franco-Salvador, Francisco Rangel, Berta Chulvi, and Paolo Rosso. Overview of autextification at iberlef 2023: Detection and attribution of machine-generated text in multiple domains. *arXiv preprint arXiv:2309.11285*, 2023. 2
- [33] Zhixiong Su, Yichen Wang, Herun Wan, Zhaohan Zhang, and Minnan Luo. Haco-det: A study towards fine-grained machine-generated text detection under human-ai coauthoring. In Wanxiang Che, Joyce Nabende, Ekaterina Shutova, and Mohammad Taher Pilehvar, editors, *Annual Meeting of the Association for Computational Linguistics (ACL)*, pages 22015–22036. ACL, 2025. 2
- [34] Zhen Sun, Zongmin Zhang, Xinyue Shen, Ziyi Zhang, Yule Liu, Michael Backes, Yang Zhang, and Xinlei He. Are we in the ai-generated text world already? quantifying and monitoring AIGT on social media. In Wanxiang Che, Joyce Nabende, Ekaterina Shutova, and Mohammad Taher Pilehvar, editors, *Annual Meeting of the Association for Computational Linguistics (ACL)*, pages 22975–23005. ACL, 2025. 2, 4, 11
- [35] Hugo Touvron, Thibaut Lavril, Gautier Izacard, Xavier Martinet, Marie-Anne Lachaux, Timothée Lacroix, Baptiste Rozière, Naman Goyal, Eric Hambro, Faisal Azhar, et al. Llama: Open and efficient foundation language models. *arXiv preprint arXiv:2302.13971*, 2023. 4
- [36] Hugo Touvron, Louis Martin, Kevin Stone, Peter Albert, Amjad Almahairi, Yasmine Babaei, Nikolay Bashlykov, Soumya Batra, Prajjwal Bhargava, Shruti Bhosale, et al. Llama 2: Open foundation and fine-tuned chat models. *arXiv preprint arXiv:2307.09288*, 2023. 4
- [37] Eli Verwimp, Rahaf Aljundi, Shai Ben-David, Matthias Bethge, Andrea Cossu, Alexander Gepperth, Tyler L Hayes, Eyke Hüllermeier, Christopher Kanan, Dhiresha Kudithipudi, et al. Continual learning: Applications and the road forward. *arXiv preprint arXiv:2311.11908*, 2023. 2
- [38] Junchao Wu, Shu Yang, Runzhe Zhan, Yulin Yuan, Lidia S. Chao, and Derek Fai Wong. A survey on llm-generated text detection: Necessity, methods, and future directions. *Comput. Linguistics*, 51(1):275–338, 2025. 1, 2

- [39] Yue Wu, Yinpeng Chen, Lijuan Wang, Yuancheng Ye, Zicheng Liu, Yandong Guo, and Yun Fu. Large scale incremental learning. In *Proceedings of the IEEE/CVF conference on computer vision and pattern recognition*, pages 374–382, 2019. 4
- [40] Lu Yu, Bartłomiej Twardowski, Xialei Liu, Luis Herranz, Kai Wang, Yongmei Cheng, Shangling Jui, and Joost van de Weijer. Semantic drift compensation for class-incremental learning. In *Proceedings of the IEEE/CVF conference on computer vision and pattern recognition*, pages 6982–6991, 2020. 2
- [41] Xiao Yu, Yi Yu, Dongrui Liu, Kejiang Chen, Weiming Zhang, Nenghai Yu, and Jing Shao. Evobench: Towards real-world llm-generated text detection benchmarking for evolving large language models. In Wanxiang Che, Joyce Nabende, Ekaterina Shutova, and Mohammad Taher Pilehvar, editors, *Findings of the Association for Computational Linguistics: ACL*, pages 14605–14620. ACL, 2025. 2
- [42] Da-Wei Zhou, Zi-Wen Cai, Han-Jia Ye, De-Chuan Zhan, and Ziwei Liu. Revisiting class-incremental learning with pre-trained models: Generalizability and adaptivity are all you need. *International Journal of Computer Vision*, 133(3):1012–1032, 2025. 4
- [43] Da-Wei Zhou, Hai-Long Sun, Han-Jia Ye, and De-Chuan Zhan. Expandable subspace ensemble for pre-trained model-based class-incremental learning. In *Proceedings of the IEEE/CVF Conference on Computer Vision and Pattern Recognition*, pages 23554–23564, 2024. 4
- [44] Fei Zhu, Xu-Yao Zhang, Chuang Wang, Fei Yin, and Cheng-Lin Liu. Prototype augmentation and self-supervision for incremental learning. In *Proceedings of the IEEE/CVF conference on computer vision and pattern recognition*, pages 5871–5880, 2021. 4

A Sufficiency Analysis of Frozen Representations

Since *RidgeFT* freezes the task-tuned encoder during the incremental stage, a natural question arises: do frozen representations still preserve discriminative information for future generators? To answer this question, we compare three feature spaces derived from the same frozen encoder: the raw representation $h = f_{\theta}(x)$, the covariance-calibrated representation $\tilde{h} = P_{\delta}(h - \mu)$, and the random feature representation $z = \text{LN}(\text{ReLU}(R\tilde{h}))$. We diagnose these feature spaces using nearest-centroid probes and ridge probes, where none of the methods updates the encoder parameters.

This analysis is conducted under the P5 protocol, where the model is first trained on five initial classes and GPT-4o-mini is introduced as the final new generator. As shown in Table 4, applying a ridge probe directly on the raw frozen representation h already yields a new-class F1 of 0.844, which suggests that the frozen encoder is not limited to the initial classes and still preserves useful discriminative cues for subsequent

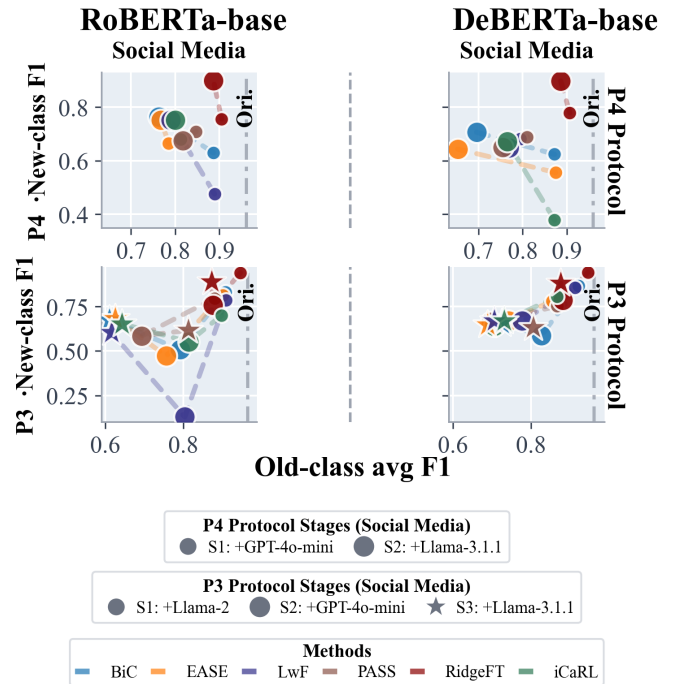


Figure 6: Lifelong MGT attribution experiments on the social media topic. P3 starts with three initial classes and sequentially adds Llama-2, GPT-4o-mini, and Llama-3.1; P4 starts with four initial classes and sequentially adds GPT-4o-mini and Llama-3.1.

Table 4: Sufficiency analysis of frozen representations. All methods use the same frozen encoder. Ridge on h already achieves a relatively strong new-class F1, suggesting that the frozen representation retains discriminative information for future generators. *RidgeFT* further improves performance, indicating that covariance calibration and random feature mapping can exploit this information more effectively.

Probe on frozen-encoder features	Full-F1	Old-F1	New-F1
Nearest-centroid on h	0.788	0.847	0.495
Nearest-centroid on z	0.854	0.879	0.730
Ridge on h	0.887	0.895	0.844
<i>RidgeFT</i> on z	0.892	0.899	0.860

generators. Building on this, *RidgeFT* further improves the new-class F1 to 0.860, while also maintaining stable old-class F1. On the other hand, the nearest-centroid probe improves from 0.495 on h to 0.730 on z , indicating that the feature transformations in *RidgeFT* make the class structure more suitable for statistic-based analytic classification.

It should be noted that this analysis does not imply that a frozen encoder is always sufficient for arbitrary future generators. The random feature mapping can only enhance the usability of the information already present in the frozen representation, but it cannot recover generator-specific information that is entirely absent from the encoder. Therefore, *RidgeFT* is better suited to scenarios where the frozen representation still provides at least partial coverage of future generators. For generators that are extremely out of distribution, periodic adaptation of the encoder may still be necessary.

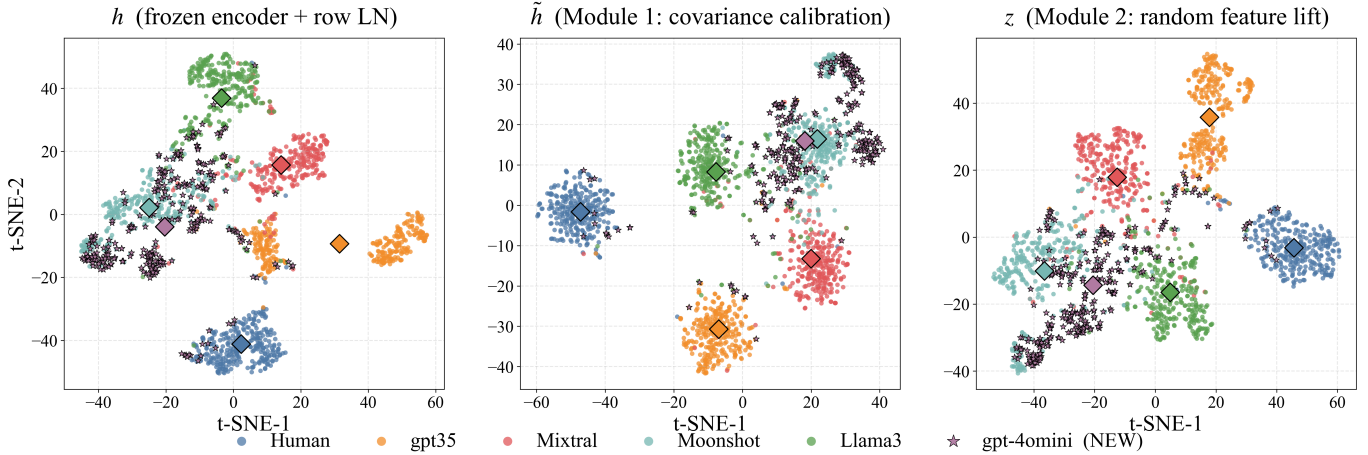


Figure 7: t-SNE visualization of different frozen feature spaces. We compare the raw frozen representation h , the calibrated representation \tilde{h} , and the random feature representation z . The figure shows that the newly introduced generator does not completely collapse into the old classes, and that the feature transformations in *RidgeFT* make the class structure more clearly separated (STEM / DeBERTa-base / P5 setting).

B Artifact Licenses, Intended Use, and Data Safety

We use two publicly released benchmark datasets, MGT-Academic [21] and AIGTBench [34], and do not collect any new user data. MGT-Academic is released under the MIT license, and AIGTBench is released under the Apache 2.0 license. Both datasets are released for research on machine-generated or AI-generated text detection/attribution, and our use is consistent with their intended research purposes. We cite the original datasets and papers, and we do not redistribute the raw datasets as part of this work.

For privacy and content safety, we use the processed benchmark versions released by the original authors. These datasets have already undergone preprocessing and moderation by their respective creators. Our experiments only use text content and class labels for aggregate model training and evaluation, and we do not analyze, expose, or redistribute any individual-level information.

C Software Implementations and Package Settings

All experiments were conducted in a Linux environment with kernel version 5.4.0-174-generic and Python 3.12.2. We used PyTorch 2.10.0+cu128 with CUDA 12.8 on an NVIDIA L20 GPU with driver version 550.54.15. Transformer encoders and tokenizers were implemented with HuggingFace Transformers 4.57.6, using DeBERTa-v3-base and RoBERTa-base as the main backbones. Encoder fine-tuning followed a unified configuration with a maximum sequence length of 256, batch size 16, 3 training epochs, AdamW optimization, weight decay, and gradient clipping.

Traditional machine learning classifiers and evaluation metrics were implemented with scikit-learn 1.7.2. Numerical computation relied on NumPy 2.0.1 and SciPy 1.15.2, while result aggregation and visualization used Pandas 2.2.3 and Matplotlib 3.9.1. For *RidgeFT*, we fixed the main hyperpa-

rameters across all primary experiments: fractional whitening exponent $\delta = 0.5$, shrinkage coefficient $\alpha = 0.05$, random feature dimension $d_\phi = 4096$, ridge regularization coefficient $\lambda = 1.0$, and class-balanced ridge coefficient $\beta = 1.0$. Each experiment was run three times, and we report the average results.

D Computational Experiments

We report the computational cost of different update strategies on a single NVIDIA L20 GPU. Under the P5 protocol with DeBERTa-v3-base, *RidgeFT* updates the classifier by recomputing sufficient statistics and solving a closed-form ridge regression problem, which only takes a few seconds for the newly added generator. In contrast, the joint-from-scratch baseline retrains an 184M-parameter DeBERTa-v3-base model on all old and new training texts, involving about 94k samples, and takes approximately 50 minutes on a single GPU. The initial five-class encoder training is shared across methods and takes 1,738 seconds.

These results show that *RidgeFT* achieves much lower incremental update cost than full retraining, while avoiding access to old raw texts during the update stage. This efficiency advantage is central to our lifelong MGT attribution setting, where attribution systems must incorporate newly emerging generators without repeatedly retraining the entire model.

E Use of AI Assistants

We used AI assistants only for language polishing, grammar checking, and improving the readability of the manuscript. All research ideas, experimental designs, implementation decisions, experimental results, analyses, and final claims were developed, checked, and approved by the authors. The AI assistants were not used to independently generate, validate, or interpret experimental results, and they are not listed as authors.

Table 5: New-class F1 across Domains and Models (final continual step). * denotes methods using data replay. Darker color indicates better performance. Bold values are the highest among continual-learning methods of the RoBERTa and DeBERTa blocks in each row. The “Ori.” column is marked “—” because no new class has been introduced at S0.

Domain	New Model	RoBERTa-base								DeBERTa-base							
		Ori.	LwF*	iCaRL*	BiC*	EASE*	PASS	SimpleCIL	RidgeFT (Ours)	Ori.	LwF*	iCaRL*	BiC*	EASE*	PASS	SimpleCIL	RidgeFT (Ours)
Social Science	GPT-3.5	—	0.709	0.730	0.701	0.741	0.591	0.435	0.804	—	0.678	0.648	0.634	0.446	0.611	0.478	0.785
	Mixtral	—	0.667	0.684	0.677	0.665	0.621	0.356	0.760	—	0.632	0.652	0.630	0.420	0.592	0.399	0.750
	Moonshot	—	0.675	0.679	0.655	0.557	0.590	0.477	0.738	—	0.644	0.658	0.646	0.473	0.590	0.430	0.740
	Llama-3.1	—	0.592	0.591	0.572	0.618	0.560	0.332	0.716	—	0.457	0.555	0.486	0.395	0.541	0.347	0.742
	GPT-4o-mini	—	0.676	0.662	0.721	0.696	0.591	0.546	0.808	—	0.713	0.718	0.710	0.705	0.646	0.481	0.830
	Average	—	0.664	0.669	0.665	0.655	0.591	0.429	0.765	—	0.625	0.646	0.621	0.488	0.596	0.427	0.769
STEM	GPT-3.5	—	0.767	0.761	0.751	0.737	0.610	0.460	0.857	—	0.690	0.707	0.677	0.665	0.615	0.459	0.845
	Mixtral	—	0.724	0.728	0.693	0.719	0.637	0.424	0.804	—	0.722	0.708	0.686	0.711	0.614	0.476	0.825
	Moonshot	—	0.751	0.710	0.747	0.746	0.663	0.512	0.823	—	0.766	0.771	0.760	0.768	0.660	0.609	0.839
	Llama-3.1	—	0.666	0.582	0.629	0.589	0.612	0.432	0.787	—	0.677	0.669	0.625	0.673	0.616	0.519	0.821
	GPT-4o-mini	—	0.798	0.784	0.800	0.644	0.661	0.567	0.871	—	0.731	0.756	0.792	0.813	0.681	0.556	0.881
	Average	—	0.741	0.713	0.724	0.687	0.637	0.479	0.829	—	0.717	0.722	0.708	0.726	0.637	0.524	0.842
Humanities	GPT-3.5	—	0.806	0.805	0.794	0.815	0.684	0.496	0.867	—	0.713	0.756	0.741	0.738	0.652	0.525	0.858
	Mixtral	—	0.645	0.628	0.610	0.632	0.612	0.420	0.696	—	0.615	0.604	0.575	0.558	0.589	0.423	0.690
	Moonshot	—	0.661	0.665	0.635	0.636	0.589	0.542	0.709	—	0.644	0.643	0.634	0.630	0.596	0.557	0.723
	Llama-3.1	—	0.525	0.607	0.518	0.543	0.587	0.416	0.693	—	0.567	0.509	0.530	0.515	0.560	0.441	0.735
	GPT-4o-mini	—	0.733	0.741	0.752	0.743	0.652	0.480	0.827	—	0.686	0.632	0.693	0.682	0.667	0.364	0.823
	Average	—	0.674	0.689	0.662	0.674	0.625	0.471	0.758	—	0.645	0.629	0.635	0.625	0.612	0.462	0.766
AIGTBench	GPT-3.5	—	0.678	0.646	0.674	0.643	0.667	0.363	0.745	—	0.720	0.708	0.660	0.705	0.676	0.468	0.755
	GPT-4o-mini	—	0.701	0.558	0.678	0.580	0.732	0.507	0.789	—	0.682	0.696	0.598	0.685	0.690	0.494	0.775
	Llama-1	—	0.903	0.851	0.917	0.922	0.810	0.845	0.960	—	0.877	0.873	0.878	0.882	0.772	0.625	0.943
	Llama-2	—	0.751	0.708	0.748	0.724	0.650	0.409	0.867	—	0.730	0.769	0.746	0.763	0.638	0.574	0.862
	Llama-3.1	—	0.780	0.758	0.815	0.794	0.735	0.487	0.907	—	0.743	0.678	0.715	0.756	0.663	0.557	0.894
	Average	—	0.763	0.704	0.766	0.733	0.719	0.522	0.853	—	0.750	0.745	0.719	0.758	0.688	0.543	0.846
Overall Average	—	0.710	0.694	0.704	0.687	0.643	0.475	0.801	—	0.684	0.685	0.671	0.649	0.633	0.489	0.806	

Table 6: Old-class F1 across domains and models (final incremental step, initial-class subset). * denotes methods using data replay. Darker color indicates better performance. Bold values indicate the best result among continual-learning baselines within each RoBERTa-base and DeBERTa-base block. The “Ori.” column reports the S0 macro-F1 on the initial classes, which is identical to full-F1 because all classes are old at S0.

Domain	New Model	RoBERTa-base								DeBERTa-base							
		Ori.	LwF*	iCaRL*	BiC*	EASE*	PASS	SimpleCIL	RidgeFT (Ours)	Ori.	LwF*	iCaRL*	BiC*	EASE*	PASS	SimpleCIL	RidgeFT (Ours)
Social Science	GPT-3.5	0.906	0.858	0.868	0.861	0.864	0.808	0.836	0.877	0.891	0.847	0.845	0.835	0.814	0.814	0.822	0.864
	Mixtral	0.938	0.881	0.868	0.886	0.881	0.837	0.854	0.905	0.938	0.883	0.866	0.873	0.826	0.824	0.848	0.903
	Moonshot	0.931	0.881	0.875	0.877	0.868	0.818	0.855	0.893	0.922	0.873	0.863	0.864	0.850	0.822	0.847	0.886
	Llama-3.1	0.920	0.865	0.849	0.863	0.850	0.801	0.835	0.882	0.912	0.850	0.837	0.844	0.824	0.792	0.818	0.875
	GPT-4o-mini	0.905	0.860	0.840	0.862	0.832	0.804	0.839	0.879	0.898	0.859	0.844	0.846	0.854	0.825	0.822	0.874
	Average	0.920	0.869	0.860	0.870	0.859	0.814	0.844	0.887	0.912	0.862	0.851	0.852	0.834	0.815	0.831	0.881
STEM	GPT-3.5	0.946	0.905	0.903	0.909	0.892	0.841	0.874	0.925	0.942	0.878	0.879	0.891	0.883	0.847	0.869	0.919
	Mixtral	0.964	0.920	0.914	0.914	0.904	0.869	0.886	0.933	0.966	0.911	0.911	0.912	0.898	0.853	0.891	0.938
	Moonshot	0.959	0.924	0.914	0.920	0.912	0.877	0.893	0.934	0.958	0.918	0.908	0.914	0.916	0.869	0.902	0.932
	Llama-3.1	0.959	0.889	0.896	0.895	0.790	0.848	0.875	0.925	0.956	0.896	0.889	0.897	0.893	0.847	0.883	0.928
	GPT-4o-mini	0.942	0.906	0.901	0.902	0.808	0.859	0.879	0.921	0.945	0.879	0.883	0.909	0.903	0.868	0.886	0.927
	Average	0.954	0.909	0.906	0.908	0.861	0.859	0.881	0.928	0.953	0.896	0.894	0.905	0.899	0.857	0.886	0.929
Humanities	GPT-3.5	0.903	0.864	0.866	0.838	0.872	0.842	0.837	0.884	0.898	0.849	0.838	0.853	0.844	0.814	0.816	0.876
	Mixtral	0.954	0.898	0.899	0.899	0.893	0.857	0.882	0.912	0.952	0.874	0.872	0.891	0.887	0.846	0.864	0.906
	Moonshot	0.936	0.889	0.874	0.885	0.885	0.817	0.860	0.893	0.945	0.861	0.866	0.882	0.862	0.828	0.866	0.902
	Llama-3.1	0.928	0.866	0.839	0.863	0.863	0.808	0.842	0.882	0.922	0.727	0.843	0.848	0.844	0.774	0.834	0.880
	GPT-4o-mini	0.903	0.865	0.855	0.867	0.857	0.828	0.829	0.876	0.905	0.859	0.769	0.857	0.831	0.833	0.804	0.877
	Average	0.925	0.876	0.867	0.870	0.874	0.831	0.850	0.889	0.924	0.834	0.838	0.866	0.853	0.819	0.837	0.888
AIGTBench	GPT-3.5	0.964	0.915	0.915	0.916	0.907	0.875	0.892	0.924	0.959	0.903	0.874	0.903	0.880	0.864	0.883	0.920
	GPT-4o-mini	0.956	0.847	0.888	0.903	0.844	0.879	0.882	0.918	0.954	0.821	0.862	0.881	0.825	0.840	0.864	0.912
	Llama-1	0.913	0.890	0.870	0.893	0.891	0.859	0.884	0.906	0.916	0.882	0.869	0.872	0.872	0.859	0.828	0.904
	Llama-2	0.918	0.877	0.838	0.876	0.860	0.824	0.848	0.897	0.919	0.867	0.854	0.878	0.861	0.825	0.859	0.899
	Llama-3.1	0.915	0.881	0.858	0.865	0.846	0.856	0.835	0.897	0.913	0.860	0.779	0.865	0.853	0.823	0.844	0.895
	Average	0.933	0.882	0.874	0.890	0.869	0.859	0.868	0.908	0.932	0.867	0.848	0.880	0.858	0.842	0.856	0.906
Overall Average	0.933	0.884	0.877	0.885	0.866	0.840	0.861	0.903	0.930	0.865	0.857	0.876	0.861	0.833	0.853	0.901	